ION

A Station-Specific Ionospheric Modeling Method for the Estimation and Analysis of BeiDou-3 Differential Code Bias Parameters

Ningbo Wang[1*] | **Zishen Li[1]** | **Andrzej Krankowski[2]** | **Xingliang Huo[3]**

[1] Aerospace Information Research Institute (AIR), Chinese Academy of Sciences (CAS), Beijing 100094, China

[2] Space Radio-Diagnostics Research Centre, University of Warmia and Mazury in Olsztyn, 10-720 Olsztyn, Poland

[3] State Key Laboratory of Geodesy and Earth's Dynamics, Innovation Academy of Precision Measurement Science and Technology (APM), CAS, Wuhan 430077, China

Correspondence

*Ningbo Wang, Aerospace Information Research Institute (AIR), Chinese Academy of Sciences (CAS), Beijing 100094, China
Email: N. Wang (wangningbo@aoe.ac.cn)

Abstract

A modified generalized trigonometric series (GTS) function is presented for the joint estimation of local ionospheric activities and differential code biases (DCBs) of the third-generation BeiDou navigation satellite system (BeiDou-3). Using observational data from the iGMAS and IGS-MGEX networks, DCBs between the pilot-, data- and I-components of BeiDou-3 signals are estimated and analyzed for January 2019. The stability of the modified GTS-based satellite DCB estimates an improvement of about 29.7% compared to the original GTS-based results. In comparison with transmitted T_{GDB1Cp} and T_{GDB2ap} parameters, the consistency between broadcast and post-processed biases reaches 0.33 and 0.50 ns. The estimated data-pilot biases are observed to be notably smaller than BeiDou-3 transmitted inter-signal correction (ISC) parameters. In the analysis of receiver B1I-B3I, DCBs generated from the independent BeiDou-2 and BeiDou-3 constellations, the receiver-type dependent biases are emphasized, which raises the consideration of using receiver-group specific bias concept in the future estimation of BeiDou DCBs.

Keywords

BeiDou-3 global system, data-pilot bias, differential code bias (DCB), inter-signal correction (ISC), station-specific ionospheric modeling

1 | INTRODUCTION

The second-generation BeiDou navigation satellite system (BeiDou-2), which employs a mixed constellation of *geostationary Earth orbits* (GEO), *inclined geosynchronous orbits* (IGSO), and *medium Earth orbits* (MEO), has provided regional positioning and navigation services in the Asia-pacific region since late December 2012 (Montenbruck et al., 2013; Yang et al., 2014). The BeiDou-2 constellation is compromised of a total of 15 operational satellites, out of which five are GEO satellites, six are IGSO satellites, and three are MEO satellites. To expand the regional BeiDou-2 into the third-generation BeiDou global system (BeiDou-3), the BeiDou-3 demonstration system (BeiDou-3S), which is constituted of two satellites in IGSOs and three satellites in MEOs, was constructed from 2015 to 2016 to verify the newly designed navigation signals (Xiao et al., 2016), inter-satellite links

(Tang et al., 2018), and onboard frequency standards (Wu et al., 2018) of the future BeiDou-3 system (Yang et al., 2018).

With the completion of BeiDou-3S, 18 BeiDou-3 satellites have been launched into MEOs, and one BeiDou-3 satellite was launched into a GEO from 2017 to 2018. The preliminary global service of BeiDou-3 started in late December of 2018 with 18 operational BeiDou-3 MEO satellites, out of which 10 were manufactured by the China Academy of Space Technology (CAST), and the others by the Shanghai Engineering Center for Microsatellites (SECM). The full constellation of BeiDou-3 now includes three GEO satellites, three IGSO satellites, and 24 MEO satellites; all of which have provided the operational capability of global service since July of 2020 (Yang et al., 2020).

Different from the Global Positioning System (GPS) and Galileo, BeiDou refers its broadcast clock offsets to the single-frequency B3I signal. For BeiDou-2, two *timing group delay* (TGD) parameters, i.e., T_{GD1} (= B1I-B3I) and T_{GD2} (= B2I-B3I), were provided to account for the *differential code biases* (DCBs) between B1I/B2I and B3I signals. In the network-based GNSS DCB estimation, satellite and receiver DCBs are commonly determined to be a by-product of global or regional ionospheric total electron content (TEC) modeling or estimated from the code differences after accounting for satellite-to-receiver ionospheric path delays (Sanz et al., 2017; Sardón et al., 1994).

The first category of DCB estimation is reliant on the thin-shell or multi-layer ionospheric assumption, in which DCB parameters are modeled as constant unknowns in the mathematical algorithms (e.g., spherical harmonics or polynomials) for ionospheric TEC calculation (Hernández-Pajares et al., 1999; Li et al., 2014, 2021; Vergados et al., 2016). This method is also employed by the GNSS control segment itself for the estimation of broadcast TGD parameters, but aligned to a calibrated reference receiver (e.g., GPS) or satellite (e.g., BeiDou) before transmission. The second category of DCB estimation requires the use of a priori ionospheric information, among which *global ionospheric maps* (GIMs) provided by the International GNSS Service (IGS) are generally employed. The estimation of receiver DCBs is more complicated due to the inferior internal thermal stabilization of receiver hardware as well as the poor geographic coverage of observational data compared to satellite DCB estimation (Themens et al., 2015; Zhang et al., 2019).

With the use of multi-GNSS observations from the Multi-GNSS Experiment (MGEX) network of the IGS, BeiDou B1I/B2I-B3I DCBs are routinely generated by the German Aerospace Center (DLR; Montenbruck et al., 2014) and Chinese Academy of Sciences (CAS; Wang et al., 2016, 2020). Although different methods are continually employed by the DLR and CAS to calculate their respective BeiDou DCBs, the two DCB products exhibit root-mean-square (RMS) differences at the magnitude of 0.4 ns (Wang et al., 2016). The influence of satellite-induced pseudorange biases on BeiDou-2 DCB estimation should also be emphasized (Wanninger & Beer, 2015). As discussed in Shu et al. (2017), the day-to-day DCB variation of BeiDou-2 MEO satellites was reduced to 0.1 ns after applying code phase pattern corrections in the estimation of BeiDou-2 DCBs.

For the smooth transition from the regional BeiDou-2 to the global BeiDou-3, the backward-compatible B1I on 1,561.098 MHz and B3I on 1,268.52 MHz were transmitted as open service (OS) signals in BeiDou-3S/3. The newly designed signals modulated on the new B1 (B1C) and B2 (subdivided into B2a and B2b) frequencies partly overlap with GPS L1/L5 and Galileo E1/E5a/E5b signals. To address satellite group delays of B1C and B2a pilot components with respect to B3I signal, two additional TGD parameters (i.e., T_{GDB1Cp} and T_{GDB2ap}) were provided in BeiDou-3's

navigation messages. Two *inter-signal correction* (ISC) parameters (i.e., ISC_{B1Cd} and ISC_{B2ad}) were also introduced to account for the biases between data and pilot components of B1C and B2a signals, respectively.

The availability of BeiDou-3 observational data from MGEX and the international GNSS Monitoring and Assessment System (iGMAS) networks provides the possibility to examine the characteristics of satellite and receiver DCBs of BeiDou-3. The elevation-dependent code biases, which were commonly observed in BeiDou-2 pseudorange measurements (Wanninger & Beer, 2015), remain absent in B1I/B3I and the new signals of BeiDou-3S/3 satellites (Zhou et al., 2018). The improved data quality and the absence of satellite-induced pseudorange biases in BeiDou-3 signals is sure to benefit DCB estimation as well as the associated standard and precise applications of BeiDou-3.

The purpose of this research is to report an adjusted station-specific ionospheric modeling method to estimate the new DCBs between pilot-, data- and I-components of BeiDou-3 signals, which also provides an update on the generation of CAS multi-GNSS DCBs (Wang et al., 2016). Following this introduction, the modified local ionospheric modeling technique is presented in detail for the estimation of BeiDou satellite and receiver DCBs. Thereafter, a summary of the data used in this study is provided. The resulting BeiDou-3 DCBs from iGMAS-only, MGEX-only, and iGMAS-plus-MGEX solutions are then analyzed and discussed in the subsequent sections. Finally, a summary and conclusion are given.

2 | METHOD

Except for the intra-frequency biases (i.e., DCBs between signals on a common frequency), the determination of inter-frequency biases needs the use of an a priori ionospheric model or the joint estimation of the ionospheric and DCB parameters in local or global scales (Montenbruck et al., 2014). An adjusted station-specific ionospheric modeling method is presented here for the estimation of BeiDou-3 DCBs.

The observation equation of pseudorange measurement $P_{r,ix}^s$ of satellite s with the tracking mode x on the frequency f_i can be expressed as:

$$P_{ix}^s = \rho^s + c\left(\delta t - \delta t^s + b_{ix} + b_{ix}^s\right) + \alpha_i \cdot I^s + T^s + \varepsilon_{ix}^s \tag{1}$$

using the notation ρ^s for the geometrical distance between satellite and receiver; c for the speed of light; δt and δt^s for the receiver and satellite clock offsets; b_{ix} and b_{ix}^s for the code biases in receiver and satellite parts; α_i for the frequency-dependent factor equaling to $40.3 f_i^{-2}$; I^s for the line-of-sight ionospheric delay; T^s for the tropospheric delay; and ε_{ix}^s for the pseudorange errors comprised of multipath and thermal noise errors.

Forming a geometry-free linear combination of pseudorange measurements between tracking modes x and y of the two different frequencies f_i and f_j yields the pseudorange-based ionospheric observable:

$$\Delta P_{ij,xy}^s = \alpha_{ij} I^s + c\left(B_{ij,xy} + B_{ij,xy}^s\right) + \Delta\varepsilon_{ij,xy}^s \tag{2}$$

in which α_{ij} equals to $40.3\left(f_i^{-2} - f_j^{-2}\right)$, $B_{ij,xy}$ and $B_{ij,xy}^s$ are the associated inter-frequency biases in the receiver and satellite sides, respectively, and $\Delta\varepsilon_{ij,xy}^s$ denotes differential pseudorange errors.

Obviously, thermal noise and multipath effects are significantly amplified in pseudorange-based ionospheric observables. Although the ionospheric slant delays can be precisely extracted from dual-frequency carrier-phase measurements, they are affected by unknown integer ambiguities. There exist more precise ways to acquire ionospheric information, typically through precise point positioning (PPP) as well as its ambiguity resolution version (Liu et al., 2019; Zhang et al., 2012). In this work, the code smoothing technique is used to derive the *slant TEC* (STEC) observables (Li et al., 2014). Ignoring the smoothing errors introduced particularly by the multipath effects, the slant ionospheric delay which is biased by receiver and satellite DCBs can be re-written as:

$$\hat{S}_r^s = S_r^s + \beta\left(B_r + B^s\right) \tag{3}$$

where $\hat{S}_r^s$ and S_r^s denote the biased and bias-free STECs, respectively, and β is the frequency-dependent coefficient of DCB parameter equaling to $1/\alpha_{ij}$. Instead of ionospheric modeling on a global scale, the STEC (S_r^s) is modeled as the product of *vertical TEC* (VTEC; represented by V_r^s) under the ionospheric single-layer assumption and a mapping function $M(z)$ depending on the satellite zenith angle z at each individual GNSS station:

$$\begin{cases} S_r^s = V_r^s \cdot M(z) \\ M(z) = \left[1 - R \cdot \sin(z)/\left(R + H_{ion}\right)\right]^{-1/2} \end{cases} \tag{4}$$

where $R = 6{,}371$ km denotes the mean radius of the Earth, and $H_{ion} = 450.0$ km is the altitude of the assumed single-layer ionosphere.

A *modified generalized triangular series* (MGTS) function is thus employed for the station-specific ionospheric VTEC modeling. The VTEC value (V_r^s) at each individual station is described as the sum of the two-dimensional polynomial function of latitude and longitude and a finite Fourier series depending on the local time as follows:

$$\begin{cases} V_r^s\left(\varphi_d, \lambda_d, h\right) = \sum_{n=0}^{n_{max}} \sum_{m=0}^{m_{max}} \left\{E_{nm} \cdot \varphi_d^n \cdot \lambda_d^m\right\} + \sum_{k=0}^{k_{max}} \left\{C_k \cos(k \cdot h) + S_k \sin(k \cdot h)\right\} \\ h = 2\pi\left(t - 14\right)/T, T = 24 \text{ h} \end{cases} \tag{5}$$

in which n, m, and k are the degrees of polynomial and Fourier series functions, respectively, and E_{nm}, C_k, and S_k are the model coefficients to be estimated, while t serves as the local time. In the original *generalized trigonometric series* (GTS), the local VTEC was modeled as a function of geographic latitude and local time (Yuan & Ou, 2004). The spherical cap coordinate system is now employed instead of the geographic coordinate system in the modified GTS. The latitude φ_d and longitude λ_d in Equation (5) are calculated as:

$$\begin{cases} \varphi_d = dr \cdot \cos\varphi_c, \ \lambda_d = dr \cdot \sin\varphi_c \\ dr = \left(R + H_{ion}\right) \cdot \lambda_c \\ \varphi_c = \arccos\left[\sin\varphi_0 \cdot \sin\varphi + \cos\varphi_0 \cdot \cos\varphi \cdot \cos\left(\lambda - \lambda_0\right)\right] \\ \lambda_c = \arcsin\left[\sin\left(\lambda - \lambda_0\right) \cdot \cos\varphi/\sin\varphi_c\right] \end{cases} \tag{6}$$

using the notations (φ, λ) for the geographic latitude and longitude of the ionospheric pierce points (IPPs), (φ_0, λ_0) for the geographic latitude and longitude of

the station, and (φ_c, λ_c) for the latitude and longitude of IPPs in the spherical cap coordinate system, respectively.

The stochastic model in station-specific ionospheric modeling, which depends on satellite elevation e and local time t, is shown in Equation (7):

$$\begin{cases} W(e,t) = W(e) \cdot W(t) \\ W(e) = 1/(1 + \cos^2 e) \\ W(t) = 1 + \frac{1}{2}\left(\cos\left(\frac{t-2}{12}\pi \right) - 1 \right) \end{cases} \tag{7}$$

Such a stochastic model is expected to reduce the multipath effect, pseudorange noise, and day-night difference of the ionospheric variability on the resulting DCB estimates.

Along with BeiDou-2/3 measurements, GPS L1 and L2 data are also used to improve the quality of the station-specific ionospheric VTEC model. Based on the adjusted station-specific ionospheric modeling method at each individual station, we generated satellite-plus-receiver (SPR) DCBs covering all observed satellites and all contributing sites. While different receiver settings might cause inconsistent pseudorange biases in a GNSS network with mixed types of receivers, the most practical method in the network-based DCB estimation of GPS and BeiDou signals is to separate SPR DCBs into satellite-dependent parts and receiver-dependent parts (Hauschild & Montenbruck, 2016). For details on the generation of satellite-dependent and receiver-dependent DCBs from SPR DCBs of all stations, we refer to Wang et al. (2016).

In comparison to the original GTS function (Li et al., 2012; Yuan & Ou, 2004), the conditional number of the normal equation for MGTS-based station-specific ionospheric modeling is significantly reduced using the spherical cap coordinate system. However, the ionospheric modeling errors induced by the thin-layer model with constant height are still noteworthy. The simple thin-layer assumption was reported to be responsible for the noticeable ionospheric modeling errors in comparison to the two-shell voxel model (Hernández-Pajares et al., 1999), which are mapped into the errors of receiver DCB estimates (Juan et al., 1997).

Aside from the sensitivity of DCB estimation to the selection of different thin-shell heights, especially during high solar activities, the plasmaspheric electron content also resembles a bias in the estimated DCBs when computing bias estimation using a thin-shell assumption (Themens et al., 2015). Since we only focus on the analysis of BeiDou-3 DCBs during low solar activity periods, the ionospheric thin-shell assumption is still employed, but using an adjusted local ionospheric model and a statistical model to reduce the ionospheric residual errors on DCB estimation.

3 | DATA SETS

The estimation and analysis of BeiDou-3 DCBs was performed for the duration of January 2019. Since BeiDou-3 started the preliminary global service in late December of 2018, some iGMAS and MGEX receivers have since been updated accordingly to support the tracking of new BeiDou-3 signals. The multi-GNSS receivers and trackable BeiDou-3 signals within iGMAS and MGEX networks are summarized in Table 1, in which BeiDou carrier frequencies and observation

TABLE 1
Multi-GNSS receivers and BeiDou-3 capable pseudorange measurements within iGMAS and MGEX networks (as of January 2019).

Networks	Manufactures	Receiver types	BeiDou-3 signals				Sites
			B1C	B1	B2a	B3	
iGMAS	CETC-54	CETC-54-GMR-4016	C1P	C2I	C5P	C6I	8
		CETC-54-GMR-4011	N/A				3
	CETC-20	GNSS_GGR	N/A				7
	Unicore	UB4B0-13478	C1D	C2I	C5D	C6I	6
MGEX	Javad	JAVAD TRE_3/3 DE/G3TH	C1X	C2I	C5X	C6I	30 (9)
	Leica	LEICA GR10/25/30/50	N/A	C2I	N/A	C6I	33 (0)
	Septentrio	SEPT POLARX4/4TR/5/5TR	N/A				57 (32)
	Trimble	TRIMBLE NETR9/ALLOY	N/A				70 (18)

codes are identified by their RINEX v3.04 names. Note that the numbers in brackets denote stations supporting the simultaneous tracking of BeiDou-3 B1I+B3I dual-frequency signals.

iGMAS stations utilize geodetic-grade GNSS receivers manufactured by CETC-54/20 and Unicore, respectively. Aside from the backward-compatible B1I and B3I signals, all of the above receivers support the tracking of the new B1C and B2a signals of BeiDou-3. As the availability of multiple signal channels or modulations offers multiple design options for optimal signal tracking by the receiver manufacturers themselves, the pilot and data components of B1C/B2a signals are tracked by CETC-54/20 and Unicore receivers, respectively.

MGEX stations utilize various geodetic-grade receivers from several commercial manufacturers. As of January 2019, while about 180 MGEX receivers supported BeiDou signal tracking, only 59 of them were capable of BeiDou-3 B1I+B3I dual-frequency signals, including Septentrio POLARX5/5TR, Trimble NETR9/ALLOY, and Javad TRE_3/3 DE receivers. The data-plus-pilot components of B1C and B2a signals were trackable by some Javad TRE_3/3 DE receivers, but unfortunately, the B1C signal was incorrectly recorded in the corresponding RINEX files. As a result, the estimation of DCBs between BeiDou-3 new signals was restricted to iGMAS receivers during the test period.

The B3I signal was selected as a reference to form the DCBs of BeiDou-3, including B1I-B3I (= T_{GD1}), B1Cp-B3I (= T_{GDB1Cp}), B1Cd-B3I, B2ap-B3I (= T_{GDB2ap}), and B2ad-B3I DCBs, which follows the definition of TGD parameters as specified in BeiDou-3 interface control documents. The geographic distribution of iGMAS and MGEX receivers in support of BeiDou-3 dual-frequency signal tracking is illustrated in Figure 1. To examine the influence of different networks/receivers on the estimation of BeiDou DCBs, B1I-B3I DCBs were estimated from the iGMAS-only, MGEX-only, and iGMAS-plus-MGEX observational data, respectively.

The iGMAS-only and MGEX-only, as well as iGMAS-plus-MGEX solutions were identified by IGM, MGX, and COM in subsequent sections. The separate zero-mean constraint is also applied to BeiDou-2 and BeiDou-3 measurements, respectively, to generate the respective BeiDou receiver B1I-B3I DCBs, and to analyze the receiver DCB differences estimated from the separate BeiDou-2 and BeiDou-3 measurements. As none of the iGMAS receivers support the simultaneous tracking of the pilot and data components of BeiDou-3 signals, the analysis of BeiDou-3 data-pilot bias was performed by forming the linear combination of B1Cp/B2ap-B3I and B1Cd/B2ad-B3I DCBs.
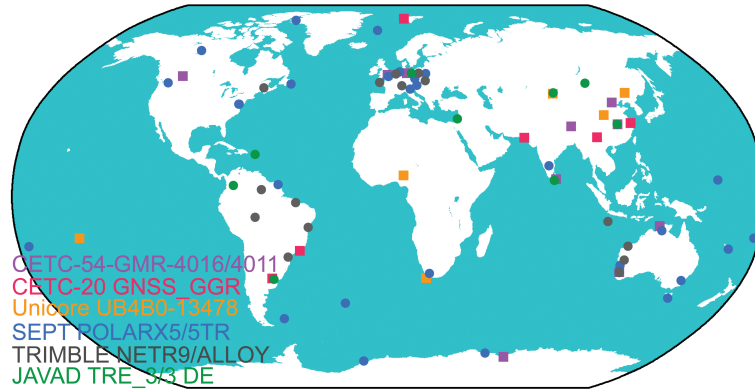
FIGURE 1 Distribution of iGMAS and MGEX stations in support of BeiDou-3 dual-frequency signal tracking. The iGMAS and MGEX receivers are identified by square and circle dots in different colors.

4 | RESULTS AND DISCUSSION

This section starts with the contribution of the modified GTS function on BeiDou DCB estimation. The variability of BeiDou-2/3 satellite B1I-B3I DCBs is then presented, followed by the analysis of receiver B1I-B3I DCB differences calculated from the independent BeiDou-2 and BeiDou-3 constellations. The analysis of BeiDou-3 new DCBs and data-pilot biases are finally performed by comparison with TGD/ISC parameters provided by the BeiDou ground control segment. Note that individual bias series have been realigned to the same reference datum to allow for direct comparison.

Based on the independent GTS and MGTS station-specific ionospheric modeling method, B1I-B3I DCBs of BeiDou-2 satellites were first calculated using MGEX receivers during the first week of 2019. Figure 2 shows the weekly standard deviations (STDs) of GTS- and MGTS-based DCB estimation results of each individual
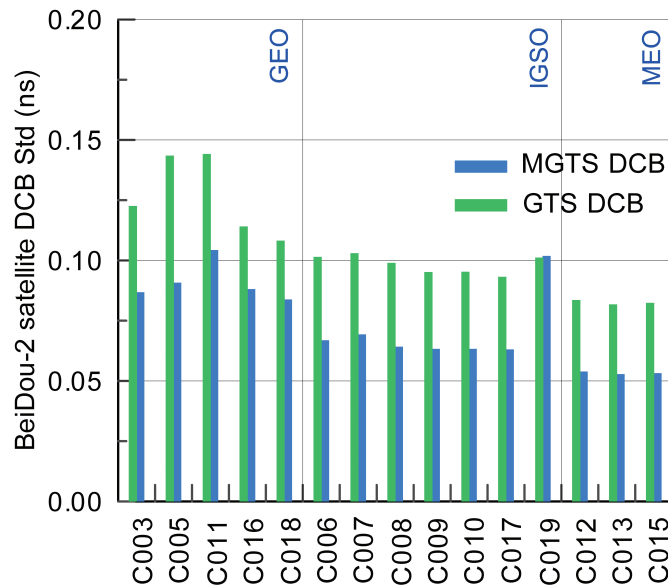
FIGURE 2 Weekly stability of BeiDou-2 satellite B1I-B3I DCBs generated by GTS-based and MGTS-based local ionospheric modeling methods

satellite. Except for the newly launched *satellite vehicle number* (SVN) C019, a pronounced improvement in the stability of satellite DCB estimates was recognized for the other satellites. For GEO satellites, the weekly STD drops from 0.13 to 0.09 ns, which decreases from 0.10/0.08 to 0.07/0.05 ns for IGSO and MEO satellites, respectively. Compared to the original GTS function, the stability of satellite DCBs improved about 29.7% across the entire BeiDou-2 constellation by applying the proposed MGTS method.

4.1 | BeiDou-2/3 B1I-B3I DCBs

The analysis of BeiDou satellite B1I-B3I DCBs from the iGMAS-only, MGEX-only, and iGMAS-plus-MGEX combined solutions are presented in this section. BeiDou-2 satellites were divided into three groups based on orbit type (i.e., GEO, IGSO, or MEO). BeiDou-3 satellites were separated into two groups according to spacecraft manufacturers (i.e., CAST and SECM).

As depicted in Figure 3, the range of B1I-B3I DCBs across the BeiDou-2 constellation varies by 25 ns. SVNs C017 and C019 show notable deviations with regard to the other BeiDou-2 satellites. As the two satellites were launched into the IGSOs in 2016 and 2018, respectively, while the others were launched before 2013, certain modifications might have been implemented on the newly launched BeiDou-2 satellites.

The range of BeiDou-3S/3 B1I-B3I DCBs, on the other hand, is around 55 ns. For BeiDou-3 satellites manufactured by CAST, two distinct DCB groups were recognized. While DCBs of the two groups differed by approximately 30 ns, the range remained only 12 ns for BeiDou-3 satellites manufactured by SECM. An ignorable difference was observed between iGMAS- and MGEX-only DCB solutions, except for certain BeiDou-2 GEO and BeiDou-3 CAST-manufactured satellites (differing by 0.3–0.7 ns). DCB differences between the MGEX-only and iGMAS-plus-MGEX solutions were within the range of 0.1 ns across the entire BeiDou constellation. No significant systematic offsets were noticed in BeiDou satellite B1I-B3I DCBs generated from the distinct networks.

To examine the stability of BeiDou-2/3 satellite DCB estimates, the day-to-day scatter, weekly, and monthly STDs of B1I-B3I DCBs from the iGMAS-only,
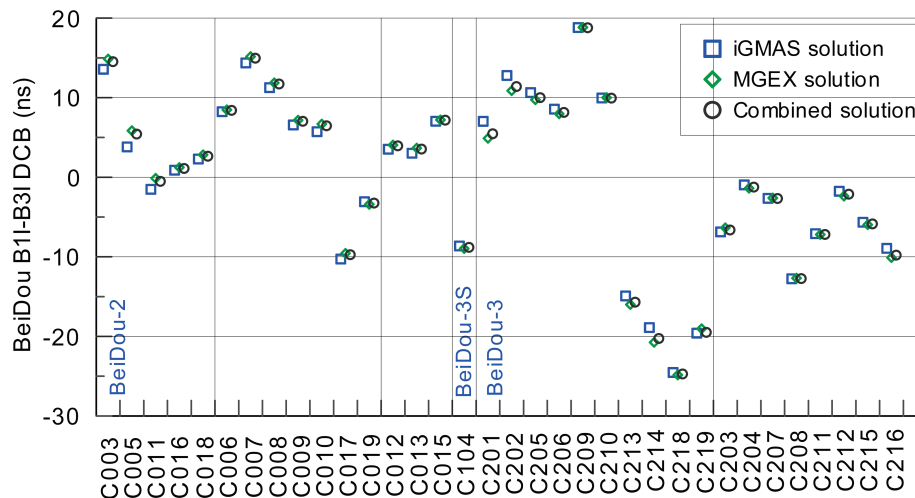

FIGURE 3 Comparison of BeiDou satellite B1I-B3I DCB estimates from the iGMAS-only, MGEX-only, and iGMAS-plus-MGEX solutions; individual satellites are identified by their SVNs.

The day-to-day repeatability as well as weekly and monthly STDs of BeiDou satellite B1I-B3I DCBs from the iGMAS-only (IGM), MGEX-only (MGX), and iGMAS-plus-MGEX (COM) solutions

Constellation		Day-to-day scatter (ns)			Weekly STD (ns)			Monthly STD (ns)		
		IGM	MGX	COM	IGM	MGX	COM	IGM	MGX	COM
BDS-2	GEO (5)	0.171	0.142	0.118	0.139	0.121	0.100	0.158	0.141	0.109
	IGSO (7)	0.072	0.119	0.088	0.056	0.082	0.062	0.082	0.100	0.074
	MEO (3)	0.156	0.164	0.158	0.128	0.150	0.138	0.137	0.154	0.131
BDS-3S	IGSO (1)	0.101	0.158	0.087	0.062	0.131	0.066	0.074	0.132	0.065
BDS-3	MEO CAST (10)	0.188	0.169	0.143	0.158	0.138	0.102	0.168	0.170	0.117
	MEO SECM (8)	0.174	0.167	0.133	0.150	0.142	0.104	0.153	0.153	0.109

MGEX-only, and iGMAS-plus-MGEX solutions are summarized in Table 2. The day-to-day scatter was calculated as the RMS of DCB differences between consecutive days across the entire test period. DCBs of BeiDou IGSO satellites exhibited notably better repeatability and stability than MEO and GEO satellites in view of the longer observation arcs and wide geographic converges of IGSO satellites.

As the satellite-induced pseudorange biases were not corrected in the estimation of BeiDou-2 DCBs, we mention here the pronounced improvement in DCB stability (15–30%) of BeiDou-2 MEO satellites after applying the code phase pattern corrections of BeiDou-2 (Shu et al., 2017). Although satellite-induced biases are proven to be absent in BeiDou-3 pseudorange measurements (Zhou et al., 2018), the DCB stability of BeiDou-3 MEO satellites is slightly worse than that of BeiDou-2 MEO satellites. The inferior DCB stability of BeiDou-3 satellites can be largely attributed to the poor BeiDou-3 B1I+B3I dual-frequency coverage of iGMAS and MGEX receivers during the test period.

The DCB repeatability and stability of the iGMAS-only solution is comparable to that of the MGEX-only solution, especially for IGSO satellites due to the good distribution of iGMAS receivers in Asia-Pacific regions. The iGMAS-plus-MGEX solution exhibited the best DCB stability performance, performing at the level of 0.121, 0.095, and 0.101 ns across the entire BeiDou constellation for the day-to-day scatter and weekly/monthly STDs, respectively. The weekly stability of BeiDou satellite DCB estimates was slightly better than the monthly stability and day-to-day repeatability. The result can be partly explained by the seven-day repeat period of BeiDou constellation, which also justifies the reasonability of providing weekly or monthly averages of DCB solutions for practical purposes.

BeiDou-transmitted T_{GD1} (= B1I-B3I) parameters are also included for comparison. Since the transmitted T_{GD1} parameters of the whole BeiDou-2/3 constellation refer to the BeiDou-2 C003 satellite, MGEX-only and iGMAS-plus-MGEX solutions were realigned to the same reference satellite. As shown in Figure 4, while a good consistency of 0.8 ns was achieved between the transmitted TGDs and post-processed DCBs for BeiDou-2, a remarkable deviation between the two products was recognized for BeiDou-3S/3 satellites.

The systematic offset between T_{GD1}-minus-$DCB_{B1I-B3I}$ differences of BeiDou-2 and BeiDou-3S/3 satellites was at the level of about 3.5 ns. One hypothesis on the inconsistency between BeiDou-2- and BeiDou-3-transmitted T_{GD1} parameters could be that independent receivers were employed by the BeiDou ground segment for the respective BeiDou-2/3 signal tracking and associated TGD calculation (Wang et al., 2019). While the origin of this "datum-deviation-like" systematic offset is presently not well explained, we noticed that the discrepancy between BeiDou-2- and BeiDou-3-transmitted T_{GD1} parameters has disappeared since late 2019.
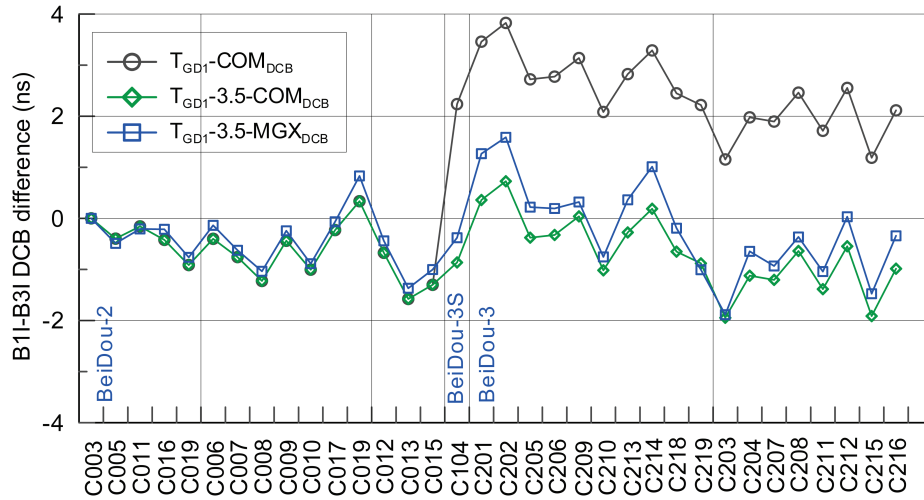
FIGURE 4 Comparison of BeiDou-transmitted T_{GD1} parameters and post-processed B1I-B3I DCBs for January 2019; MGX and COM denote DCB estimates from the MGEX-only and MGEX-plus-iGMAS solutions, respectively.
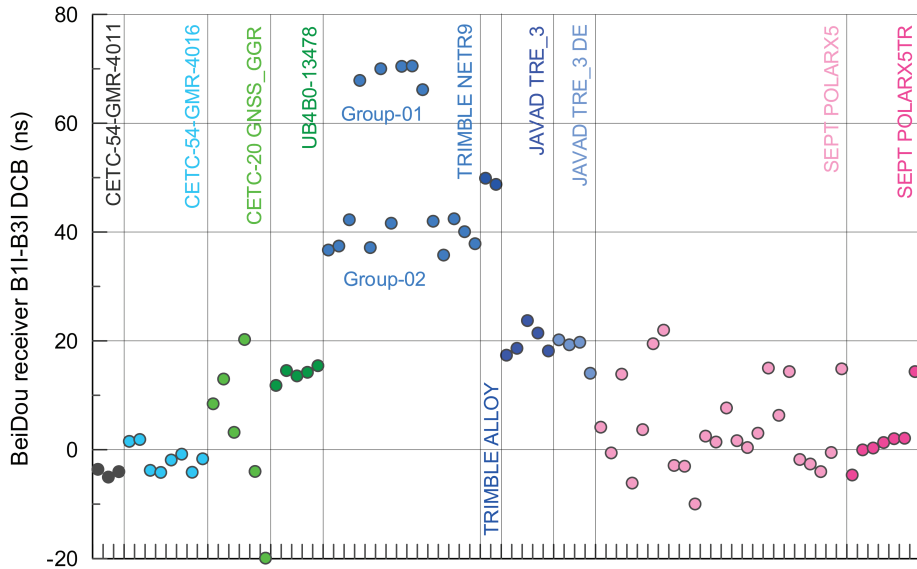

FIGURE 5 Monthly averages of BeiDou receiver B1I-B3I DCBs from the iGMAS-plus-MGEX solution

BeiDou receiver B1I-B3I DCBs from the iGMAS-plus-MGEX combined solution is shown in Figure 5. Distinct colors identify the receiver types, and the stations within individual receiver groups are sorted by their geographic locations, from high-latitudes of the southern hemisphere to high-latitudes of the northern hemisphere. For iGMAS receivers, the scatter of receiver DCBs was roughly 6.0 ns and 3.5 ns for CETC-54 and Unicore receivers, respectively. While the same firmware and antenna were employed by CETC-20 receivers, the range of the corresponding receiver DCBs reached 40 ns. For MGEX receivers, two distinct DCB groups were recognized for Trimble receivers (identified by Group-01 and Group-02). The scatter was about 4 ns for Group-01 and 6.5 ns for Group-02, respectively. Except for the two receivers employing the firmware version 5.22 (CUT000AUS) and 5.33 (KARR00AUS), the other BeiDou-3-capable Trimble NETR9/ALLOY receivers
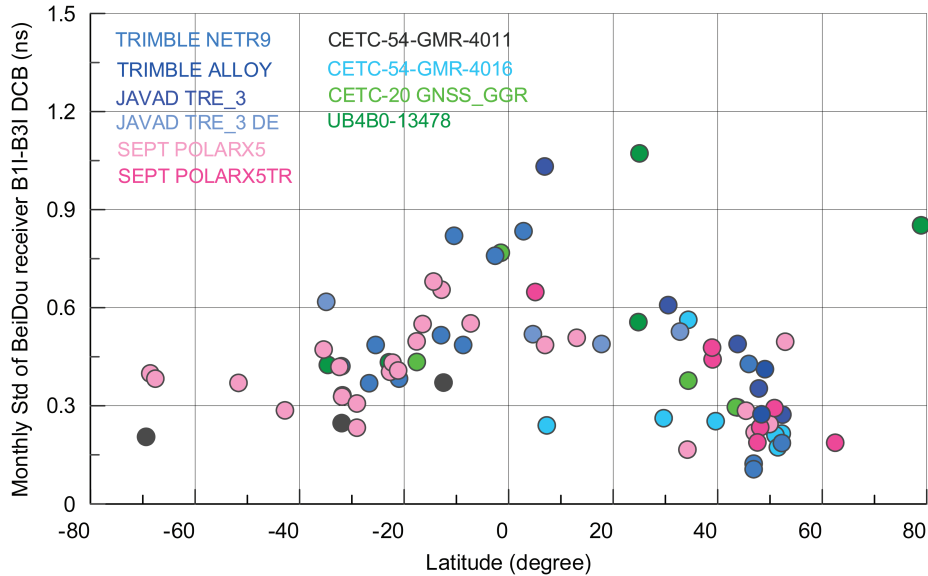
FIGURE 6   Monthly STD of BeiDou receiver B1I-B3I DCBs at the individual station

were equipped with the firmware version 5.37. This unexpected DCB deviation in Trimble receivers is currently under investigation.

The range of the Javad TRE_3 and TRE_3 DE receiver DCBs performs at the same level, which corresponds to 6.4 ns and 6 ns, respectively. The scatter of Septentrio receiver DCBs is around 30 ns, notably larger than that of Trimble Group-01/02 and Javad receivers. Since arbitrary antennas were employed at individual stations, it can merely be concluded that the variation of receiver B1I-B3I DCBs were more likely related to the receiver model itself, which showed no significant dependency on station locations. As the firmware of individual receivers has not changed over the duration of the test period, the analysis of firmware changes on the variation of receiver DCBs is not yet achievable.

The monthly STDs of receiver B1I-B3I DCBs were calculated and are depicted with respect to geographic latitudes in Figure 6. The fluctuation of BeiDou receiver DCBs is notably larger than that of satellites (see Table 2), which can be explained by the wide geographic coverage of observations in the estimation of satellite DCBs. Except for two Unicore receivers, the stability of receiver DCBs was worse for stations in equatorial and low-latitude regions than those located in mid- and high-latitude regions, which presents a site-dependent rather than receiver-dependent characteristic. The stability of receiver DCBs at different latitudes also keeps in proper accord with the magnitude of local ionospheric modeling errors, which exhibits good performance in mid-latitude regions but degraded performance in equatorial regions due to the pronounced variabilities of ionospheric gradients (Wang et al., 2017). Note that BeiDou receiver DCBs are assumed to be constant within one day in our analysis. The within-day bias variations in certain receivers might have also affected the stability of receiver DCBs (Zhang et al., 2019).

Since 15 BeiDou-2 satellites and 18 BeiDou-3 satellites were operated during the test period, the receiver B1I-B3I DCBs could be determined by independent BeiDou-2 or BeiDou-3 observations. The separate zero-mean constraint was applied to the BeiDou-2 and BeiDou-3 constellations to generate their respective DCBs and to check associated DCB differences. As shown in Figure 7, receiver DCB differences generated from the independent BeiDou-2 and Beidou-3 constellations were found to be receiver-type dependent. The scatter of receiver DCB differences was
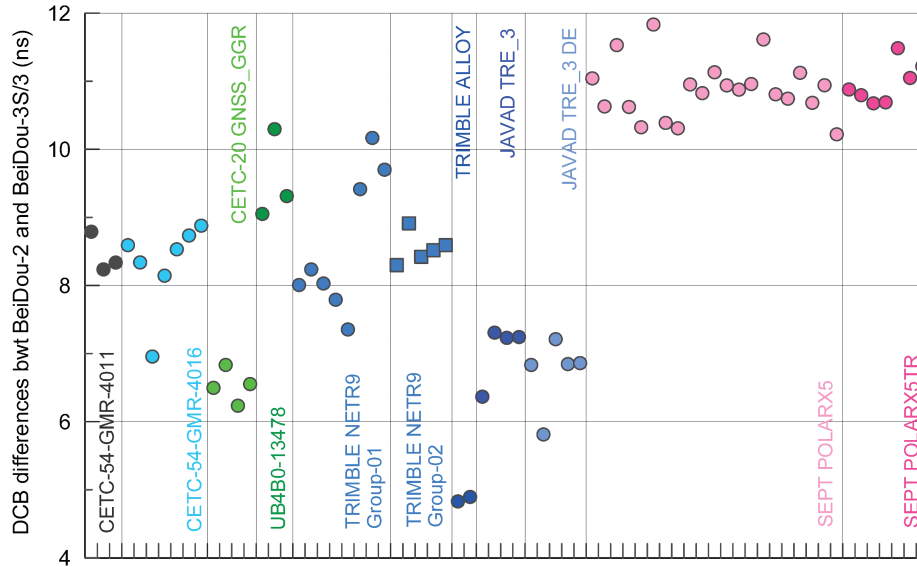
FIGURE 7 Receiver DCB differences generated from the independent BeiDou-2 and BeiDou-3 constellations; iGMAS and MGEX stations depicted on the horizontal axis are sorted by their geographic latitudes.

about 4 ns for iGMAS stations and 7 ns for MGEX stations, respectively. With the consideration of comparable scatters in receiver DCB differences, three-receiver groups could be roughly separated (i.e., CETC-54 [except for XIA3 station] plus Tremble NETR9 Group-02 receivers, CETC-20 plus Javad receivers, as well as Septentrio POLARX5/5TR receivers). The range of DCB differences proved to be about 1 ns for the first receiver group, and reached roughly 2 ns for the remaining receiver groups.

Since the BeiDou-2 constellation is comprised of satellites in different orbit types, whereas all the BeiDou-3 satellites are in MEOs during the test period, the impacts of observational data from different satellite orbit types on the resulting receiver bias estimates require further investigation. Additionally, as different options might be employed by the receiver manufacturers themselves for optimal tracking of modernized GNSS signals, the biases between different receiver types can be foreseen. The impacts of such biases would be pronounced in precise data processing of mixed receiver types.

In the analysis of receiver-satellite pair biases of BeiDou-2 pseudorange measurements, the receiver-type dependent code biases were emphasized in Gong et al. (2018). After applying the satellite and receiver-type dependent bias corrections, a remarkable improvement was reported in the estimation of BeiDou-2 satellite clock offsets and B1I+B2I dual-frequency standard positioning. Considering the receiver-type dependent biases of BeiDou pseudorange measurements (Gong et al., 2018) as well as the inferior repeatability of BeiDou DCBs in comparison to GPS and Galileo DCBs (Montenbruck et al., 2014; Wang et al., 2016), the concept of receiver-group specific biases as proposed in the Bias-SINEX format v1.0 may be considered as one option in the future estimation of BeiDou DCBs.

4.2 | BeiDou-3 New DCBs

The estimation of satellite and receiver DCBs between the data-, pilot- and I-components of BeiDou-3 signals was restricted to iGMAS receivers during the

TABLE 3

Comparison of BeiDou-3 broadcast B1C/B2a-B3I TGDs and post-processed DCBs in January 2019 (unit: ns)

Satellite		B1Cp-B3I		B1Cd-B3I	B2ap-B3I		B2ad-B3I
		T_{GDB1Cp}	DCB	DCB	T_{GDB2ap}	DCB	DCB
CAST	C201 (C19)	7.2	7.18±0.16	7.25±0.52	11.3	11.25±0.14	11.29±0.37
	C202 (C20)	14.1	14.12±0.14	13.73±0.44	11.5	11.14±0.14	10.81±0.31
	C205 (C22)	15.2	15.20±0.14	14.86±0.50	6.3	6.23±0.14	6.29±0.38
	C206 (C21)	12.9	12.97±0.16	12.71±0.53	11.2	9.87±0.15	10.72±0.32
	C209 (C23)	20.8	20.27±0.10	20.25±0.49	8.4	8.11±0.10	7.93±0.42
	C210 (C24)	15.2	14.84±0.10	14.14±0.59	7.8	7.42±0.09	7.16±0.35
	C213 (C32)	−9.5	−9.80±0.19	−9.53±0.45	6.0	5.95±0.15	5.67±0.28
	C214 (C33)	−15.9	−15.77±0.16	−16.18±0.50	−37.7	−37.42±0.29	−38.42±0.36
	C218 (C36)	−21.2	−21.77±0.14	−22.05±0.48	6.7	6.27±0.10	5.70±0.40
	C219 (C37)	−13.9	−14.38±0.14	−14.39±0.48	3.4	2.55±0.14	1.64±0.35
SECM	C203 (C27)	−4.7	−4.38±0.11	−4.26±0.43	−4.2	−3.67±0.08	−3.25±0.28
	C204 (C28)	0.0	0.29±0.15	0.47±0.46	−4.3	−3.90±0.11	−3.76±0.35
	C207 (C29)	1.6	1.97±0.14	2.01±0.44	−4.7	−4.16±0.11	−3.63±0.32
	C208 (C30)	−10.1	−9.96±0.10	−9.46±0.42	−4.9	−4.64±0.09	−4.42±0.29
	C211 (C26)	−2.8	−2.16±0.10	−1.85±0.46	−4.7	−4.05±0.11	−3.80±0.32
	C212 (C25)	−0.5	−0.43±0.09	0.11±0.51	−4.6	−4.28±0.10	−4.16±0.46
	C215 (C35)	−3.3	−3.02±0.14	−3.22±0.50	−3.2	−2.95±0.10	−2.59±0.34
	C216 (C34)	−5.2	−5.16±0.16	−4.535±0.50	−4.1	−3.72±0.11	−3.81±0.34

test period. BeiDou-3-transmitted T_{GDB1Cp} and T_{GDB2ap} parameters, which were actually DCBs between B1Cp/B2ap and B3I signals, are also included for comparison. As BeiDou-3-transmitted TGD/ISC parameters were not recorded by iGMAS receivers, those broadcast values are provided by the BeiDou ground control segment calculating from its own regional tracking network.

Broadcast TGDs, monthly averages of B1C/B2a-B3I DCBs, and their corresponding STDs of individual BeiDou-3 satellites are summarized in Table 3. All satellites are identified by their SVNs, in which SVNs C201–C219 and C203–C216 correspond to CAST- and SECM-manufactured BeiDou-3 satellites, respectively. For direct comparison purposes, all TGD and DCB values were realigned by a zero-constellation-mean adjustment to remove the reference datum differences.

Although the B1C/B2a-B3I DCBs of BeiDou-3 are calculated from a small network of iGMAS receivers, no noticeable jumps were found in the DCB series across the entire test period. For B1Cp-B3I DCBs, the range was around 42 ns for CAST-manufactured satellites and 12 ns for SECM-manufactured satellites. As for B2ap-B3I DCBs, ranges of CAST- and SECM-manufactured satellites were 50 ns and 2 ns, respectively. The DCB scatter of CAST-manufactured satellites proved to be remarkably larger than that of SECM-manufactured satellites.

The estimated B1Cp/B2ap-B3I DCBs exhibit an uncertainty (in monthly STD) of 0.13 and 0.12 ns, respectively, which are notably smaller than that of B1Cd/B2ad-B3I DCBs (0.48 and 0.35 ns). As B1C and B2a data-component signals were only supported by the Unicore receivers while the pilot-component signals were tracked by CETC-54/20 receivers, the inferior stability of B1Cd/B2ad-B3I DCBs can be partly explained by the poor B1Cd/B2ad+B3I coverage of Unicore receivers as depicted in Figure 1.

The consistency between transmitted T_{GDB1Cp} parameters and B1Cp-B3I DCBs were at the levels of 0.33 ns and 0.32 ns for CAST- and SECM-manufactured satellites, respectively, and the corresponding values were 0.54 ns and 0.43 ns between T_{GDB2ap} and $DCB_{B2ap-B3I}$. A good agreement between BeiDou-3-transmitted TGDs and post-processed DCBs was found, and no significant deviation was recognized in the B1C/2a-B3I DCBs of CAST- and SECM-manufactured satellites.

The variation of BeiDou-3 B1C/B2a-B3I receiver DCBs is depicted in Figure 8. The range of CETC-20 receiver DCBs is shown to be notably larger than DCB variations of other receiver types, reaching 30 ns and 60 ns for B1Cp-B3I and B2ap-B3I DCBs, respectively. Since the same firmware and antenna are employed by CETC-20 receivers, the reasons for the large scatter in CETC-20 receiver DCBs are currently under investigation.

Except for CETC-20 receivers, DCBs within individual receiver types exhibited similar variabilities. For CETC-54 receivers, the range was 6 ns for B1Cp-B3I DCBs and 5 ns for B2ap-B3I DCBs. For Unicore receivers, the range was 7 ns and 1 ns for B2ap-B3I and B2ap-B3I DCBs, respectively. The monthly DCB STD of Unicore receivers was in turn notably larger than that of the other two receiver types, which can also be attributed to the small number of tracking stations in the estimation of associated DCBs.

As B1C/B2a data and pilot signals could not be simultaneously tracked by iGMAS receivers, B1Cd-B1Cp and B2ad-B2ap DCBs were formed by the linear combination of $DCB_{B1Cd-B3I}$-minus-$DCB_{B1Cp-B3I}$ and $DCB_{B2ad-B3I}$-minus-$DCB_{B2ap-B3I}$, respectively. The data-pilot biases in BeiDou-3 B1C and B2a signals are depicted in Figure 9, in which a separate zero-constellation-mean condition was applied to the transmitted ISCs and post-processed DCBs. B1Cd-B1Cp and B2ad-B2ap DCBs mainly varied within the range of -0.7 to 0.6 and -1.0 to 0.8 ns, respectively. However, the corresponding values from the transmitted ISCs were significantly large, reaching from -2.4 ns to 1.6 ns and from -0.9 ns to 1.8 ns for B1C and B2a data-pilot biases, respectively.
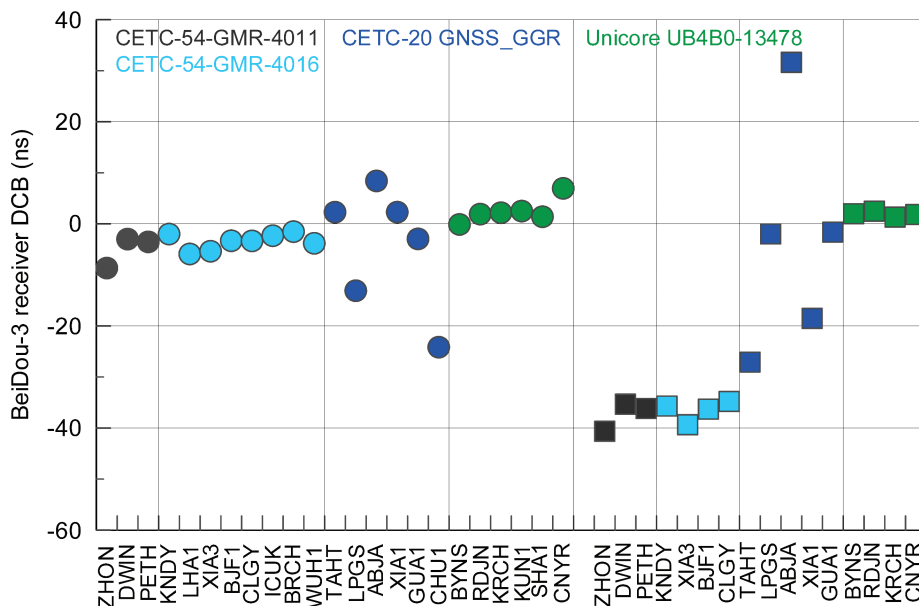
FIGURE 8 BeiDou-3 B1Cp-B3I (circle) and B2ap-B3I (square) receiver DCBs in January 2019; different types of iGMAS receivers are depicted in different colors.
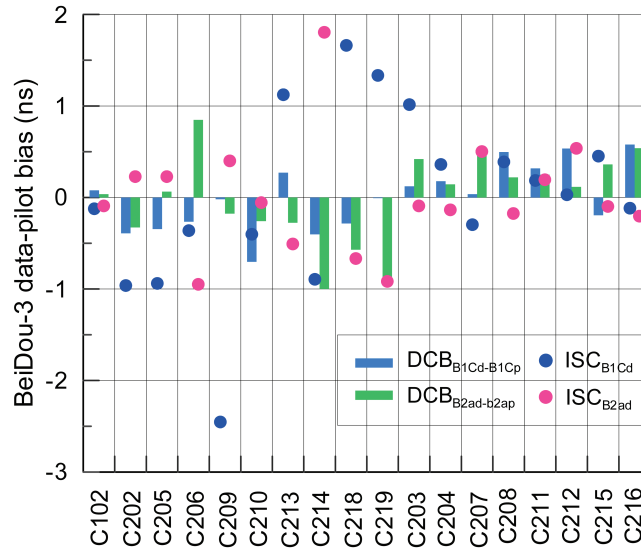
FIGURE 9 Data-pilot biases of BeiDou-3 B1C and B2a signals; the color bars and dots correspond to the post-processed DCBs and transmitted ISCs, respectively.

A good consistency between the transmitted and post-processed data-pilot biases was found for SECM-manufactured satellites, however large scatters were observed for the CAST-manufactured satellites. Considering the fact that no simultaneous tracking of BeiDou-3 data and pilot signals is currently supported by iGMAS or MGEX receivers, and that the test period corresponds to the early stage of BeiDou-3 global service, the data-pilot biases need to be further checked in the case that BeiDou-3 data and common multi-GNSS receivers could one day simultaneously track pilot signals.

5 | CONCLUSION

With the availability of BeiDou-3 observational data from iGMAS and MGEX receivers, a modified GTS function was proposed for the joint estimation of the station-specific ionospheric activities and DCB parameters between pilot-, data- and I-components of BeiDou-3 signals. The estimation and analysis of BeiDou-3 DCBs were presented over the duration of January 2019. For B1I-B3I DCBs, the monthly stability of BeiDou-3 satellite DCBs reached 0.13 ns, 0.15 ns, and 0.10 ns for the iGMAS-only, MGEX-only, and iGMAS-plus-MGEX solutions, respectively, which is comparable to that of BeiDou-2 satellites (0.13, 0.13, and 0.10 ns).

As for the new DCBs between B1Cp/B2ap and B3I signals of Beidou-3 generated from the iGMAS receivers, the monthly stability of B1Cp/B2ap-B3I DCBs was registered at 0.13 ns and 0.12 ns across the entire BeiDou-3 constellation. In comparison to T_{GDB1Cp}/T_{GDB2ap} parameters and post-processed B1Cp/B2ap-B3I DCBs, an agreement at the level of 0.33 ns and 0.50 ns was achieved. In the analysis of the linear combination of B1Cp/B2ap-B3I and B1Cd/B2ad-B3I DCBs, the data-pilot biases of BeiDou-3 B1C and B2a signals were found to be from −0.7 to 0.6 ns and from −1.0 to 0.8 ns, respectively. The poor consistency between the transmitted and estimated data-pilot biases was observed for CAST-manifested BeiDou-3 satellites, which requires further examination in case simultaneous tracking of BeiDou-3 data and pilot signals are supported by common multi-GNSS receivers.

The variation of BeiDou receiver DCBs is more likely related to the receiver model itself, but shows less dependence on station locations. The unchanged receiver firmware of individual receivers during the test period inhibited the analysis of firmware changes on the variation of receiver DCBs. The stability of receiver DCB estimates was characterized as site-dependent rather than receiver-dependent, which exhibits inferior stability for stations in equatorial and low-latitude regions but good stability for stations in mid-latitude regions.

The differences between receiver B1I-B3I DCBs generated from the independent BeiDou-2 and BeiDou-3 observational data were determined to be receiver-type dependent. The receiver B1I-B3I DCB differences reached the level of 1 to 2 ns within the individual receiver group, but increased to the magnitude of 4 to 7 ns between different receiver groups. Considering the inferior precision of BeiDou DCBs compared to GPS and Galileo DCBs, as well as the pronounced receiver-type dependent biases of BeiDou pseudorange observations, the use of receiver-group specific biases should be considered in the future estimation and analysis of BeiDou DCBs. The modified GTS function has also been used in the routine generation of CAS multi-GNSS DCBs, which are publicly downloadable from IGN and Crustal Dynamics Data Information System (CDDIS) repositories.

ACKNOWLEDGMENTS

REFERENCES

Gong, X., Lou, Y., Zheng, F., Gu, S., Shi, C., Liu, J., & Jing, G. (2018). Evaluation and calibration of BeiDou receiver-related pseudorange biases. *GPS Solutions*, *22*. https://doi.org/10.1007/s10291-018-0765-3

Hauschild, A., & Montenbruck, O. (2016). A study on the dependency of GNSS pseudorange biases on correlator spacing. *GPS Solutions*, *20*(2), 159–171. https://doi.org/10.1007/s10291-014-0426-0

Hernández-Pajares, M., Juan, J. M., & Sanz, J. (1999). New approaches in global ionospheric determination using ground GPS data. *Journal of Atmospheric And Solar-Terrestrial Physics*, *61*(16), 1237–1247. https://doi.org/10.1016/S1364-6826(99)00054-1

Hernández-Pajares, M., Roma-Dollase, D., Krankowski, A., García-Rigo, A., & Orús-Pérez, R. (2017). Methodology and consistency of slant and vertical assessments for ionospheric electron content models. *Journal Of Geodesy*, *91*(12), 1405–1414. https://doi.org/10.1007/s00190-017-1032-z

Juan, J. M., Rius, A., Hernández-Pajares, M., & Sanz, J. (1997). A two-layer model of the ionosphere using global positioning system data. *Geophysical Research Letters*, *24*(4), 393–96. https://doi.org/10.1029/97gl00092

Li, Z., Yuan, Y., Li, H., Ou, J., & Huo, X. (2012). Two-step method for the determination of the differential code biases of COMPASS satellites. *Journal Of Geodesy*, *86*(11), 1059–1076. https://doi.org/10.1007/s00190-012-0565-4

Li, Z., Yuan, Y., Fan, L., Huo, X., & Hsu, H. (2014). Determination of the differential code bias for current BDS satellites. *IEEE Transactions on Geoscience and Remote Sensing*, *52*(7), 3968–3979. https://doi.org/10.1109/tgrs.2013.2278545

Li, Z., Wang, N., Liu, A., Yuan, Y., Wang, L., Hernández-Pajares, M., Krankowski, A., & Yuan, H. (2021). Status of CAS global ionospheric maps after the maximum of solar cycle 24. *Satellite Navigation*, *2*(1). https://doi.org/10.1186/s43020-021-00050-2

Liu, T., Zhang, B., Yuan, Y., Li, Z., & Wang, N. (2019). Multi-GNSS triple-frequency differential code bias (DCB) determination with precise point positioning (PPP). *Journal Of Geodesy*, *93*(5), 765–784. https://doi.org/10.1007/s00190-018-1194-3

Montenbruck, O., Hauschild, A., Steigenberger, P., Hugentobler, U., Teunissen, P., & Nakamura, S. (2013). Initial assessment of the COMPASS/BeiDou-2 regional navigation satellite system. *GPS Solutions*, *17*, 211–222. https://doi.org/10.1007/s10291-012-0272-x

Montenbruck, O., Hauschild, A., & Steigenberger, P. (2014). Differential code bias estimation using multi-GNSS observations and global ionosphere maps. *NAVIGATION*, *61*(3), 191–201. https://doi.org/10.1002/navi.64

Sanz, J., Juan, J. M., Rovira-Garcia, A., & González-Casado, G. (2017). GPS differential code biases determination: Methodology and analysis. *GPS Solutions*, *21*(4), 1549–1561. https://doi.org/10.1007/s10291-017-0634-5

Sardón, E., Rius, A., & Zarraoa, N. (1994). Estimation of the transmitter and receiver differential biases and the ionospheric total electron content from global positioning system observations. *Radio Science*, *29*(3), 57–-586. https://doi.org/10.1029/94RS00449

Shu, B., Liu, H., Xu, L., Gong, X., Qian, C., Zhang, M., & Zhang, R. (2017). Analysis of satellite-induced factors affecting the accuracy of the BDS satellite differential code bias. *GPS Solutions*, *21*(3), 905–916. https://doi.org/10.1007/s10291-016-0577-2

Tang, C., Hu, X., Zhou, S., Liu, L., Pan, J., Chen, L., Guo, R., Zhu, L., Hu, G., Li, X., He, F., & Chang, Z. (2018). Initial results of centralized autonomous orbit determination of the new-generation BDS satellites with inter-satellite link measurements. *Journal Of Geodesy*, *92*(10), 1155–1169. https://doi.org/10.1007/s00190-018-1113-7

Themens, D. R., Jayachandran, P. T., & Langley, R. B. (2015). The nature of GPS differential receiver bias variability: An examination in the polar cap region. *Journal of Geophysical Research: Space Physics*, *120*(9), 8155–8175. https://doi.org/10.1002/2015JA021639

Vergados, P., Komjathy, A., Runge, T. F., Butala, M. D., & Mannucci, A. J. (2016). Characterization of the impact of GLONASS observables on receiver bias estimation for ionospheric studies. *Radio Science*, *51*(7), 1010–1021. https://doi.org/10.1002/2015RS005831

Wang, N., Yuan, Y., Li, Z., Montenbruck, O., & Tan, B. (2016). Determination of differential code biases with multi-GNSS observations. *Journal Of Geodesy*, *90*(3), 209–228. https://doi.org/10.1007/s00190-015-0867-4

Wang, N., Yuan, Y., Li, Z., Li, Y., Huo, X., & Li, M. (2017). An examination of the Galileo NeQuick model: Comparison with GPS and JASON TEC. *GPS Solutions*, *21*(2), 605–615. https://doi.org/10.1007/s10291-016-0553-x

Wang, N., Li, Z., Montenbruck, O., & Tang, C. (2019). Quality assessment of GPS, Galileo, and BeiDou-2/3 satellite broadcast group delays. *Advances in Space Research*, *64*(9), 1764–1779. https://doi.org/10.1016/j.asr.2019.07.029

Wang, N., Li, Z., Duan, B., Hugentobler, U., & Wang, L. (2020). GPS and GLONASS observable-specific code bias estimation: Comparison of solutions from the IGS and MGEX networks. *Journal Of Geodesy*, *94*(8). https://doi.org/10.1007/s00190-020-01404-5

Wanninger, L., & Beer, S. (2015). BeiDou satellite-induced code pseudorange variations: Diagnosis and therapy. *GPS Solutions*, *19*(4), 639–648. https://doi.org/10.1007/s10291-014-0423-3

Wu, Z., Zhou, S., Hu, X., Liu, L., Shuai, T., Xie, Y., Tang, C., Pan, J., Zhu, L., & Chang, Z. (2018). Performance of the BDS3 experimental satellite passive hydrogen maser. *GPS Solutions*, *22*(2). https://doi.org/10.1007/s10291-018-0706-1

Xiao, W., Liu, W., & Sun, G. (2016). Modernization milestone: BeiDou M2-S initial signal analysis. *GPS Solutions*, *20*(1), 125–133. https://doi.org/10.1007/s10291-015-0496-7

Yang, Y., Li, J., Wang, A., Xu, J., He, H., Guo, H., Shen, J., & Dai, X. (2014) Preliminary assessment of the navigation and positioning performance of BeiDou regional navigation satellite system. *Science China Earth Sciences*, *57*(1), 144–152. https://doi.org/10.1007/s11430-013-4769-0

Yang, Y., Xu, Y., Li, J., & Yang, C. (2018) Progress and performance evaluation of BeiDou global navigation satellite system: Data analysis based on BDS-3 demonstration system. *Science China Earth Sciences*, *61*(5), 614–624. https://doi.org/10.1007/s11430-017-9186-9

Yang, Y., Mao, Y., & Sun, B. (2020) Basic performance and future developments of BeiDou global navigation satellite system. *Satellite Navigation*, *1* (1). https://doi.org/10.1186/s43020-019-0006-0

Yuan, Y., & Ou, J. (2004) A generalized trigonometric series function model for determining ionospheric delay. *Progress in Natural Science*, *14*(11), 1010–1014. https://doi.org/10.1080/10020070412331344711

Zhang, B., Ou, J., Yuan, Y., & Li, Z. (2012) Extraction of line-of-sight ionospheric observables from GPS data using precise point positioning. *Science China Earth Sciences*, *55*(11), 1919–1928. https://doi.org/10.1007/s11430-012-4454-8

Zhang, B., Teunissen, P. J. G., Yuan, Y., Zhang, X., & Li, M. (2019). A modified carrier-to-code leveling method for retrieving ionospheric observables and detecting short-term temporal variability of receiver differential code biases. *Journal Of Geodesy*, *93*(1), 19–28. https://doi.org/10.1007/s00190-018-1135-1

Zhou, R., Hu, Z., Zhao, Q., Li, P., Wang, W., He, C., Cai, C., & Pan, Z. (2018). Elevation-dependent pseudorange variation characteristics analysis for the new-generation BeiDou satellite navigation system. *GPS Solutions*, *22*(3). https://doi.org/10.1007/s10291-018-0726-x